Geophysical Research Letters

Supporting Information for

Surface-atmosphere decoupling prolongs cloud lifetime under warm advection due to reduced entrainment drying

Haipeng Zhang[1], Youtong Zheng[2, 3], Seoung Soo Lee[1], Zhanqing Li[1]

[1]Department of Atmospheric and Oceanic Science & Earth System Science Interdisciplinary Center, University of Maryland, College Park, MD, USA

[2]Program in Atmospheric and Oceanic Sciences, Princeton University, Princeton, NJ, USA

[3]Department of Atmospheric and Earth Science, University of Houston, Houston, TX, USA

Contents of this file

Text S1. Calculations of different heights, inversion jumps, and entrainment rate

1. Inversion-top height (z_i^+), inversion-base height (z_i^-), and inversion jumps

The top and base heights of the inversion layer are calculated based on the profile of the variance of liquid water potential temperature (θ_l) following Yamaguchi & Randall (2008):

$z_i^+ = z$, where $\overline{\theta_l'^2} = 0.05 \cdot \max(\overline{\theta_l'^2})$ and $z > z_{max}$, (1a)

$z_i^- = z$, where $\overline{\theta_l'^2} = 0.05 \cdot \max(\overline{\theta_l'^2})$ and $z < z_{max}$. (1b)

z_{max} is calculated as $z_{max} = z$, where $\overline{\theta_l'^2} = \max(\overline{\theta_l'^2})$. We use linear interpolation to determine z_i^+ and z_i^- between grid levels.

Inversion jumps of moisture and temperature are thus defined as:

$\Delta q_t = q_t(z_i^+) - q_t(z_i^-)$, (2a)

$\Delta \theta_l = \theta_l(z_i^+) - \theta_l(z_i^-)$. (2b)

2. Cloud-base height (z_b), cloud-top height (z_t), and inversion height (z_i)

Following van der Dussen et al. (2016), z_b is defined as the minimum height where the cloud fraction is greater than 0.4, and z_t is defined as z_i^+ because the LWP budget analysis is performed up to the top of the inversion layer.

When used in the LWP budget, z_i is defined as z_i^+ because the evaluation of turbulent fluxes at this height yields the best closure of the LWP budget, as suggested by van der Dussen et al. (2016). Otherwise, z_i is defined as the height of the maximum potential temperature vertical gradient in a conventional way.

3. Entrainment rate (w_e)

The entrainment rate (w_e) is determined by the boundary-layer mass budget equation:

$w_e = \frac{dz_i}{dt} - w_{sub}(z_i)$, (3)

where z_i is the boundary-layer height, and $w_{sub}(z_i)$ is the large-scale subsidence rate at the top of the boundary layer.

Text S2. Robustness of the results to simulation settings

Simulation settings (i.e., domain size, grid spacing, and cloud microphysical schemes) might influence our main result that decoupling prolongs the cloud lifetime. For example, the domain size used might be too small to simulate mesoscale circulations that affect stratocumulus transitions. The variations in vertical resolution near the PBL inversion influence the simulation of the entrainment rate, a crucial variable that impacts the cloud lifetime. The selection of specific cloud microphysics schemes may also affect our results due to their impacts on precipitation. **Figures S13-16** examine the robustness of the results to these settings. We find that the main result holds well. The entrainment rate under cold-advection conditions is somewhat sensitive to the domain size, whereas those under warm-advection conditions are relatively insensitive (Figure S13). The same is true for perturbed horizontal or vertical resolutions. We also find that the LWP is affected by microphysics schemes, especially under warm-advection conditions (Figure S15). Even though the modeling results are different in response to changes in these simulation settings, it is still clear that MBL clouds persist longer under warm-advection conditions than under cold-advection conditions (Figures S13 and S15). The physical mechanisms that the interplay of entrainment drying and cloud-base turbulent moisture transport determines cloud lifetime stay the same (Figures S14 and S16).

Table S1. Description of the supplementary sensitivity runs.

Simulation	Description	Objective
BaseRun	CADV and WADV, with default KK2000 scheme. They serve as base runs for the sensitivity experiments below.	To examine the cloud response to warm-advection-induced decoupling
dDIV	Decrease the large-scale divergence rate from $5.0 \times 10^{-6}\ s^{-1}$ to $-1.0 \times 10^{-6}\ s^{-1}$	To examine the impact of environmental conditions on the conclusion
vDIV	Allow the large-scale divergence rate to co-vary with SST, with its relationship determined from ERA5 reanalysis data (see Figure S2)	
dQT	Decrease the free-tropospheric total water mixing ratio by 30%	
iINV	Increase the initial temperature jump across the inversion by 5.5 K	
Diurnal	Allow diurnal cycle of insolation	To examine the impact of diurnal cycle on the conclusion
LargeDom	Increase the domain size from 4.2 km to 20.16 km	To examine the impact of simulation settings on the conclusion
HiResHoriz	Double the horizontal resolution	
HiResVert	Refine the vertical resolution near the inversion from 5 m to 3 m	
MP_M2005	Use the M2005 microphysics scheme instead	
MP_P3	Use the P3 microphysics scheme instead	
MP_THOM	Use the THOM microphysics scheme instead	

Note: KK2000 is a simplified (drizzle only) version of the Khairoutdinov & Kogan (2000) microphysics scheme used for conversion between cloud and rainwater as well as raindrop evaporation and sedimentation; M2005 is the Morrison et al. (2005) double-moment microphysics scheme; P3 is the predicted particle properties scheme (Morrison & Milbrandt, 2015); THOM is the Thompson et al. (2008) microphysics scheme.

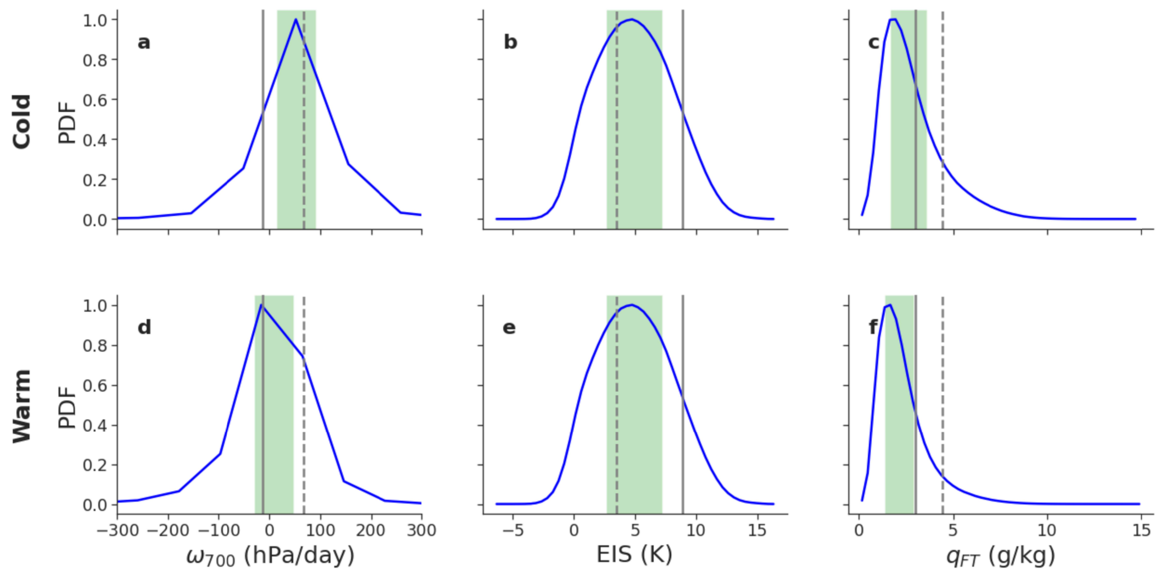

Figure S1. Normalized PDFs of daily **(a)** vertical velocity at 700 hPa, **(b)** estimated inversion strength, and **(c)** free-tropospheric humidity (defined as the water vapor mixing ratio averaged between 700 hPa and 850 hPa) under cold-advection conditions in mid-latitude stratocumulus regions (i.e., low-cloud fraction > 0.5), derived from 2003-2018 ERA5 reanalysis data (meteorological factors; Hersbach et al., 2020) and CERES Edition 4A Single Scanner Footprint products (low-cloud fraction; Minnis et al., 2021). **(d-f)** are the same as (a-c) but under warm-advection conditions. Green areas cover the interquartile range. Dashed lines show initial values specified in the base runs (WADV/CADV), with solid lines for sensitivity runs (dDIV/dQT/iINV).

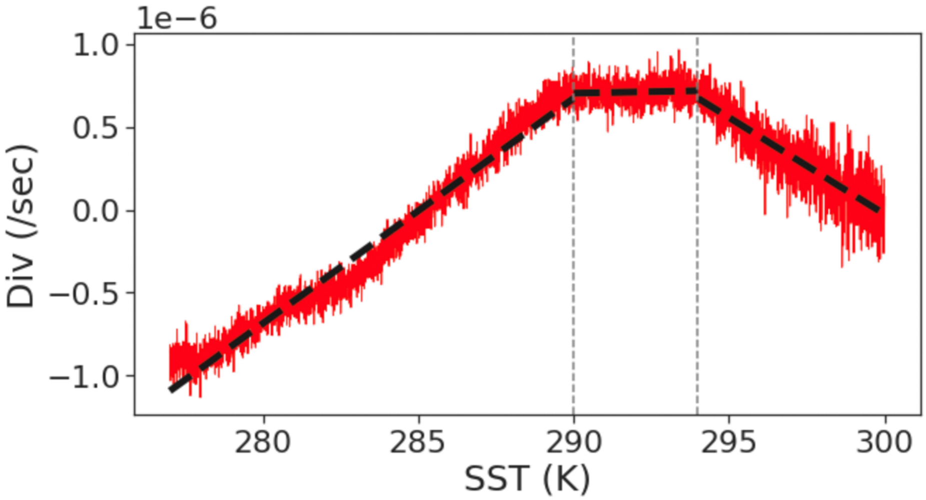

Figure S2. Large-scale divergence rate (Div) as a function of sea surface temperature (SST), derived from 2003-2018 daily ERA5 reanalysis data. The black dashed line is the fitted regression line used to determine the varying divergence rate in the sensitivity run vDIV.

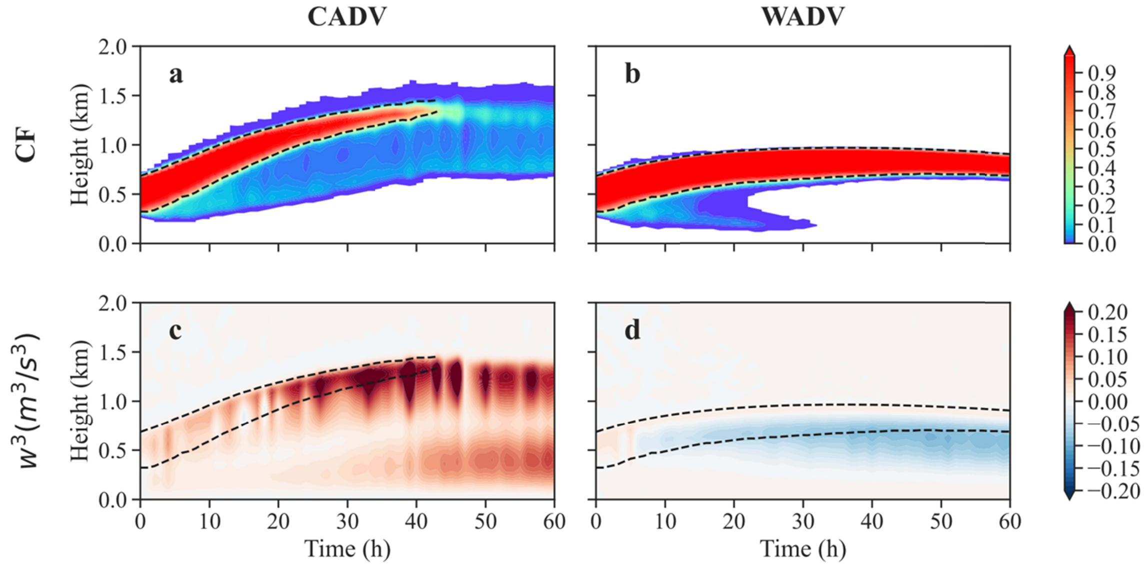

Figure S3. Time-height plots of **(a)** cloud fraction and **(c)** the skewness of the vertical velocity for CADV, with **(b)** and **(d)** for WADV. Dashed lines show the inversion height (defined as the height of the maximum potential temperature vertical gradient) and the cloud-base height, respectively.

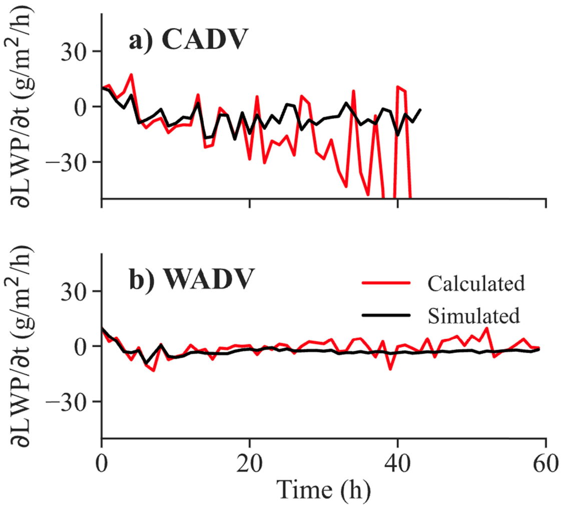

Figure S4. Time series of the calculated LWP tendency (i.e., the sum of five budget terms; red) and the simulated LWP tendency (black) from **(a)** CADV and **(b)** WADV.

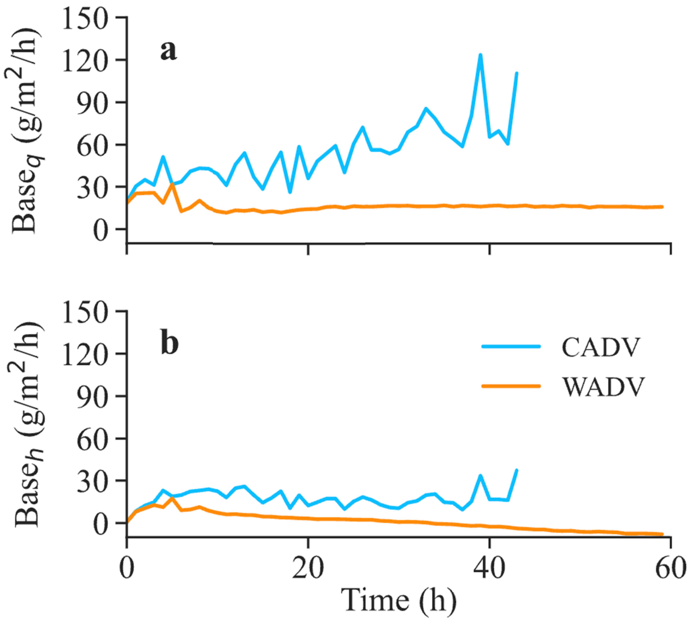

Figure S5. Time series of the LWP tendency due to cloud-base turbulent fluxes consisting of **(a)** moisture fluxes and **(b)** heat fluxes.

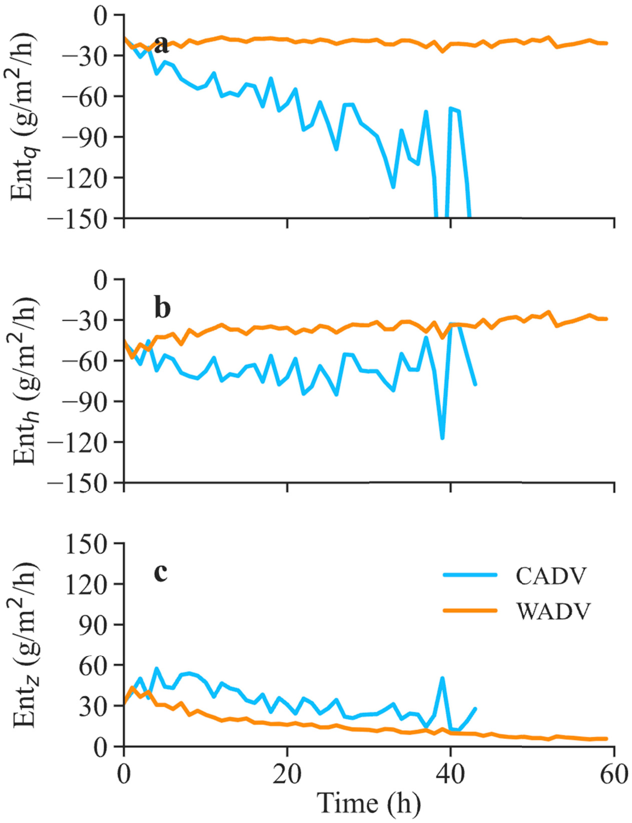

Figure S6. Time series of the LWP tendency due to entrainment effects consisting of **(a)** entrainment drying, **(b)** entrainment warming, and **(c)** entrainment-induced cloud deepening.

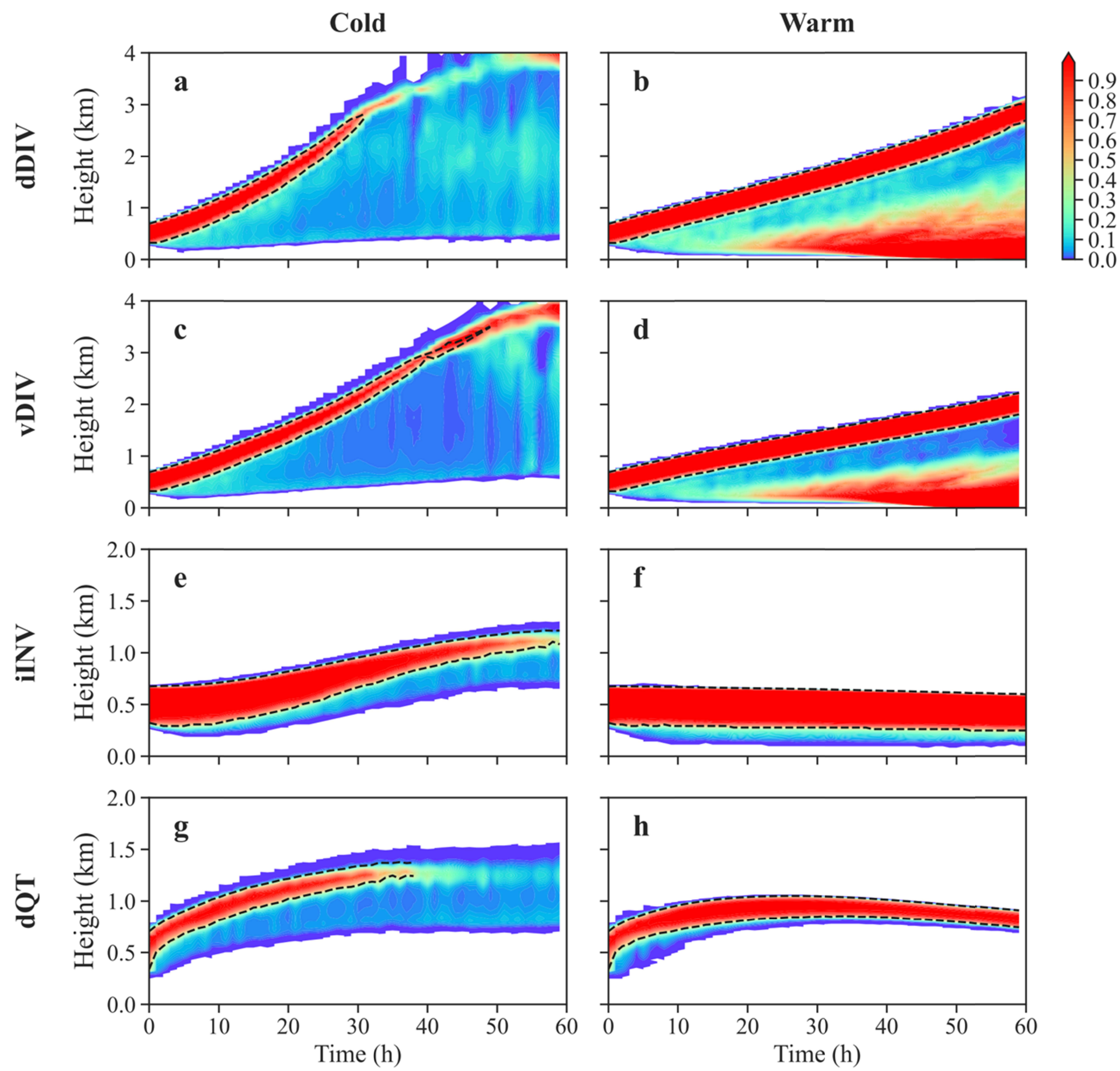

Figure S7. Time-height plots of cloud fraction under cold-advection conditions (left column) and warm-advection conditions (right column) for sensitivity runs dDIV, vDIV, iINV, and dQT (upper to lower rows, respectively). Dashed lines show the inversion height (defined as the height of the maximum potential temperature vertical gradient) and the cloud-base height, respectively.

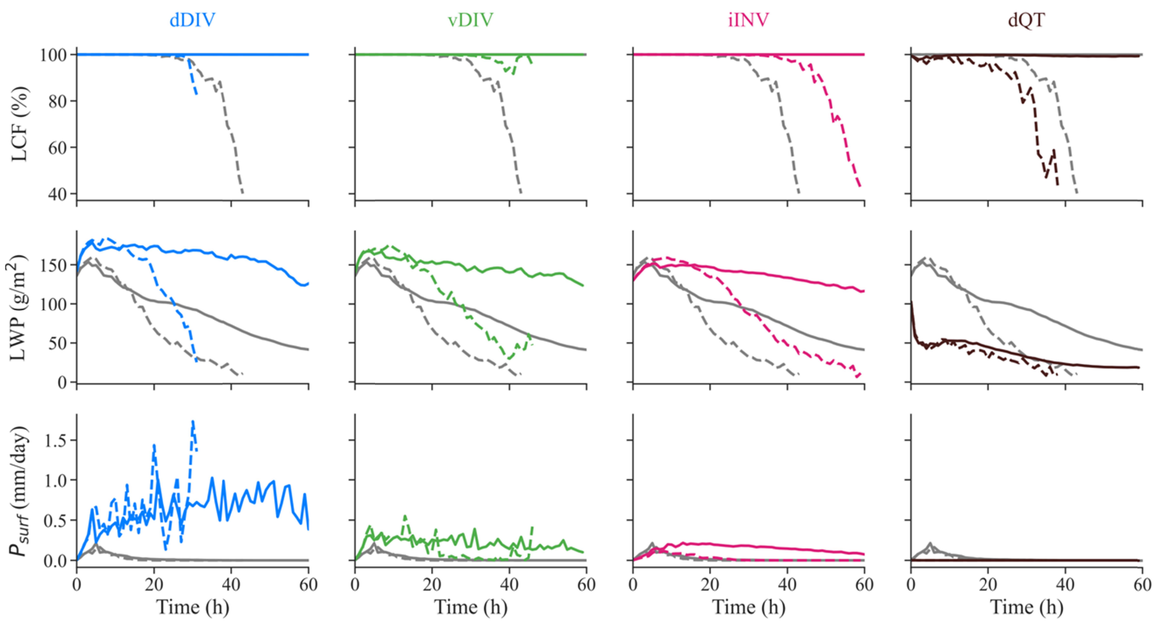

Figure S8. Time series of low-cloud fraction, cloud liquid water path, and precipitation at the surface (upper to lower rows, respectively) for sensitivity runs dDIV, vDIV, iINV, and dQT (left to right columns, respectively). Solid and dashed lines represent warm-advection cases and cold-advection cases, respectively. Grey lines represent base runs (WADV/CADV).

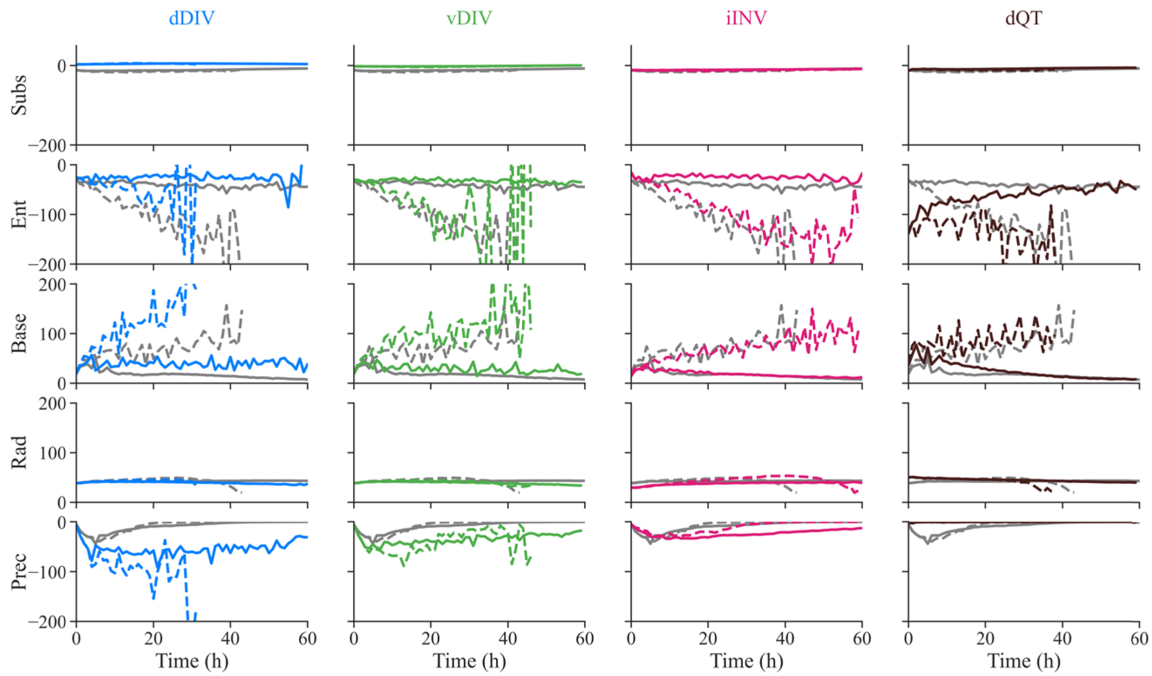

Figure S9. Same as Figure S8, but for time series of the LWP tendency ($g/m^2/h$) due to large-scale subsidence (*Subs*), entrainment (*Ent*), cloud-base turbulent fluxes (*Base*), radiation (*Rad*), and precipitation (*Prec*) (upper to lower rows, respectively).

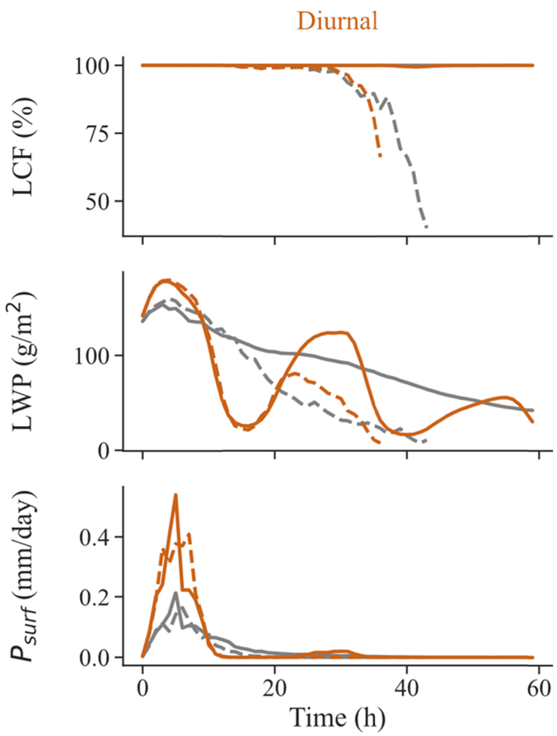

Figure S10. Same as Figure 8, but for the sensitivity run Diurnal.

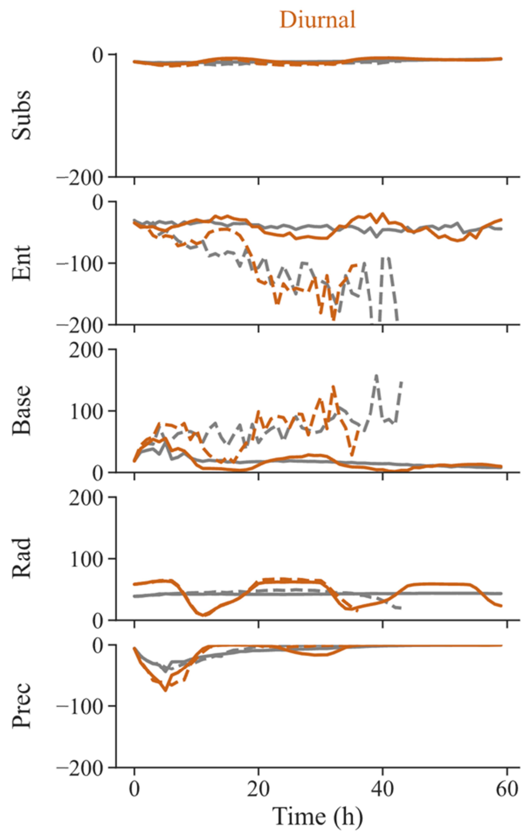

Figure S11. Same as Figure 8, but for the sensitivity run Diurnal.

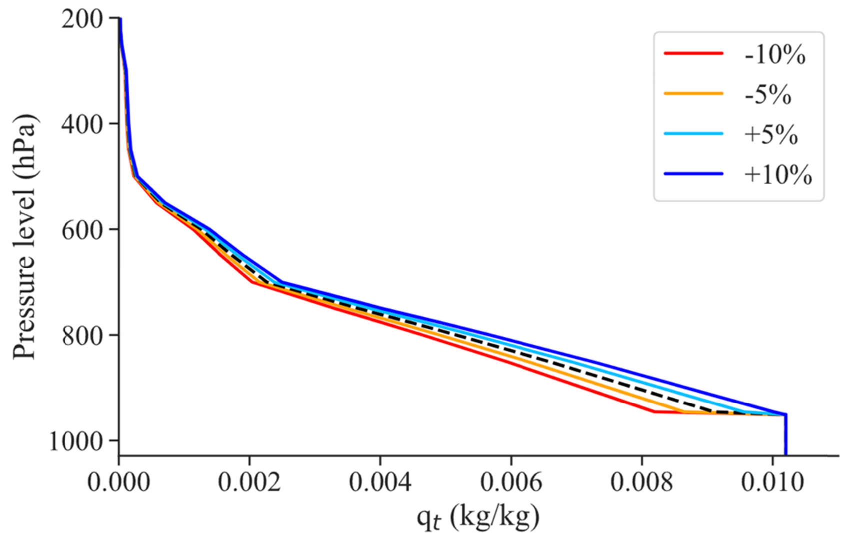

Figure S12. Initial total water mixing ratio profiles for sensitivity experiments CADV_FTMs/WADV_FTMs. The black dashed line is the moisture profile for control experiments (CADV/WADV).

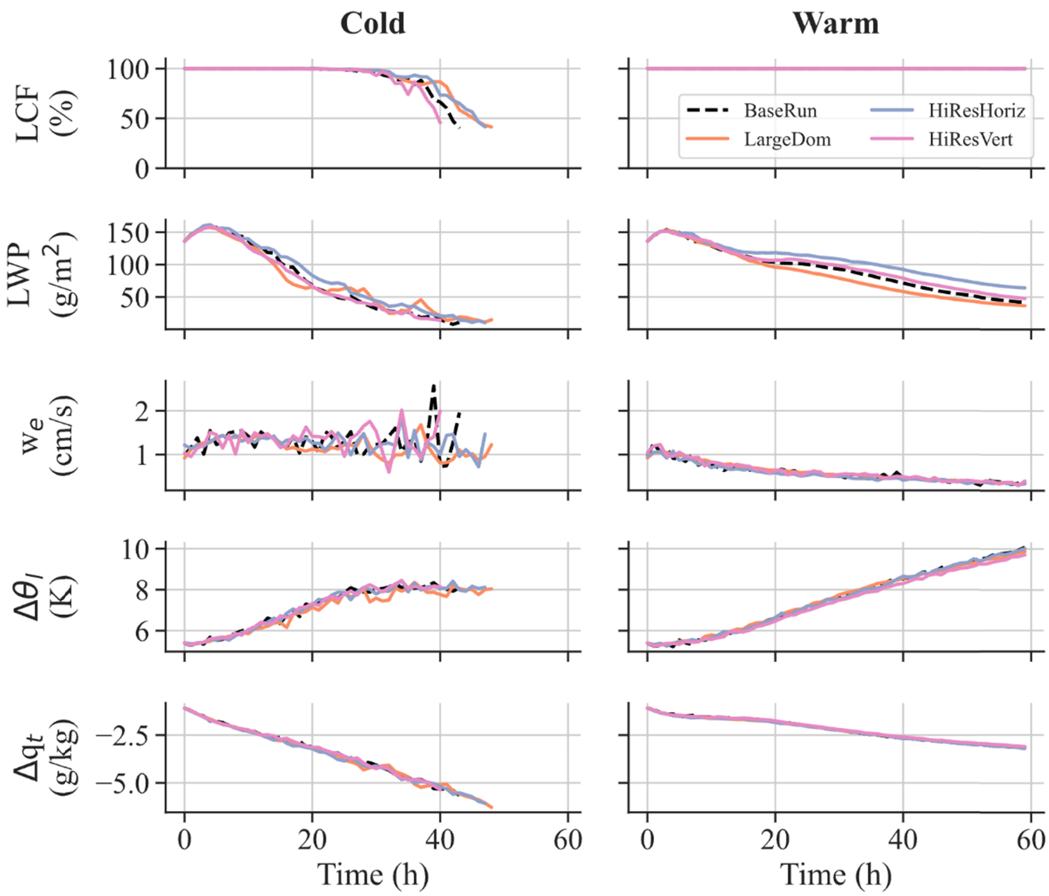

Figure S13. Time series of low-cloud fraction, liquid water path, entrainment rate, inversion temperature jump, and inversion moisture jump (upper to lower rows, respectively) for experiments BaseRun, HiResHoriz, LargeDom, and HiResVert under cold-advection conditions (left column) and warm-advection conditions (right column).

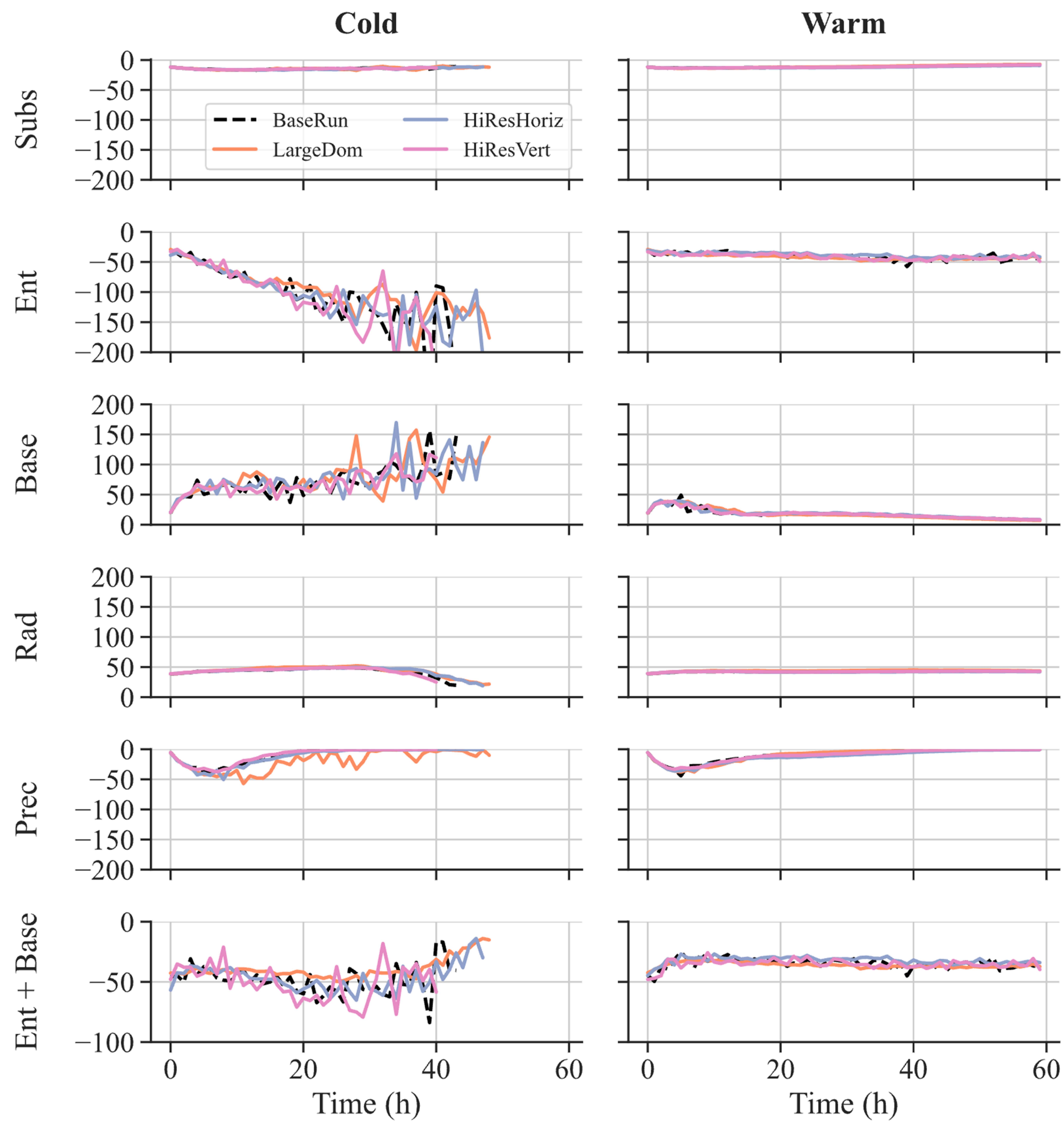

Figure S14. Same as Figure S13, but for time series of the LWP tendency (g/m^2/h) due to large-scale subsidence (*Subs*), entrainment (*Ent*), cloud-base turbulent fluxes (*Base*), radiation (*Rad*), precipitation (*Prec*), and the sum of *Ent* and *Base* (upper to lower rows, respectively).

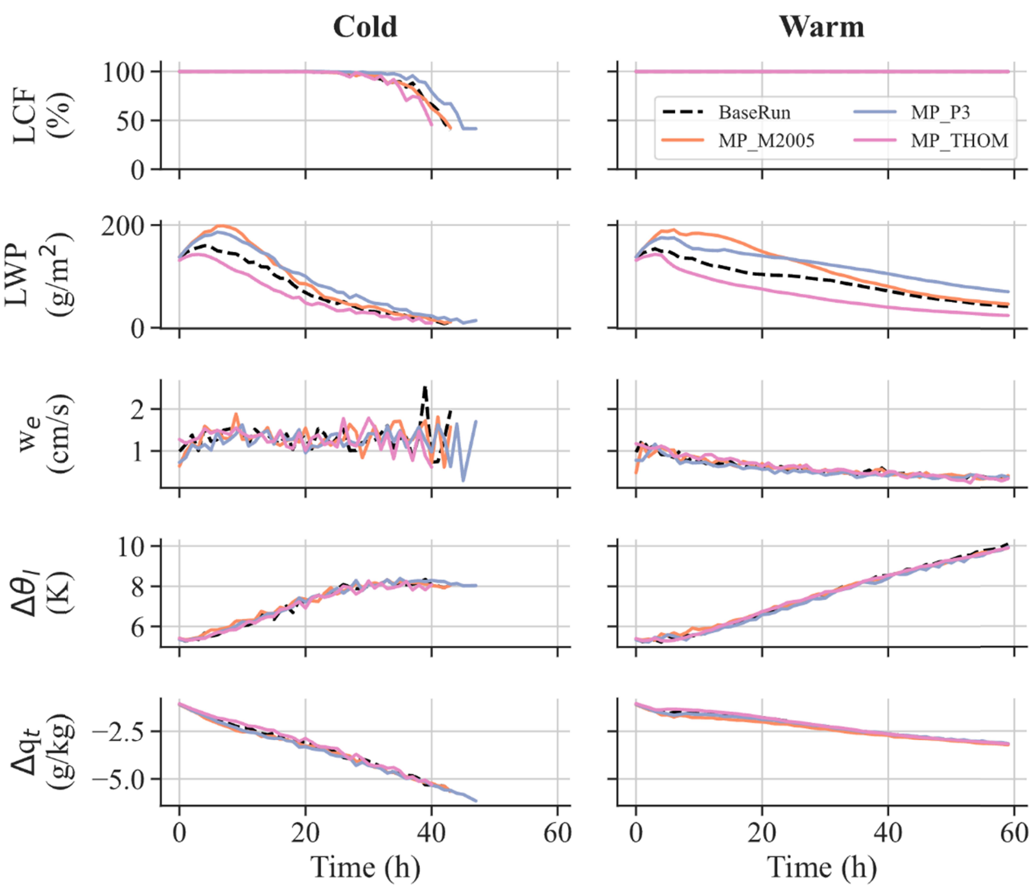

Figure S15. Time series of low-cloud fraction, liquid water path, entrainment rate, inversion temperature jump, and inversion moisture jump (upper to lower rows, respectively) for experiments BaseRun, MP_M2005, MP_P3, and MP_THOM under cold-advection conditions (left column) and warm-advection conditions (right column).

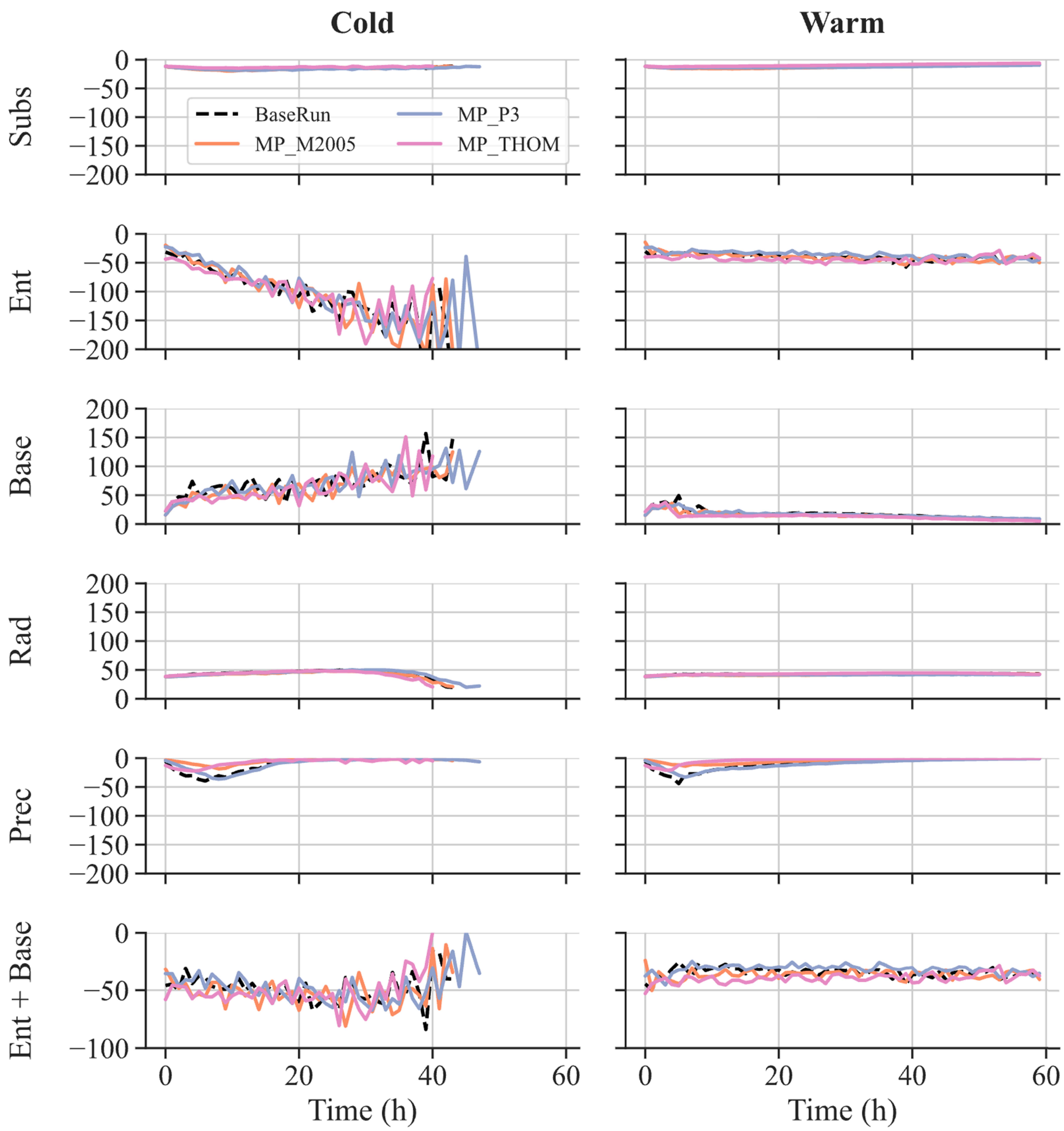

Figure S16. Same as Figure S15, but for time series of the LWP tendency (g/m^2/h) due to large-scale subsidence (*Subs*), entrainment (*Ent*), cloud-base turbulent fluxes (*Base*), radiation (*Rad*), precipitation (*Prec*), and the sum of *Ent* and *Base* (upper to lower rows, respectively).

References

van der Dussen, J. J., de Roode, S. R., & Siebesma, A. P. (2016). How large-scale subsidence affects stratocumulus transitions. *Atmospheric Chemistry and Physics*, *16*(2), 691–701. https://doi.org/10.5194/acp-16-691-2016

Hersbach, H., Bell, B., Berrisford, P., Hirahara, S., Horányi, A., Muñoz-Sabater, J., et al. (2020). The ERA5 global reanalysis. *Quarterly Journal of the Royal Meteorological Society*, *146*(730), 1999–2049. https://doi.org/10.1002/qj.3803

Khairoutdinov, M., & Kogan, Y. (2000). A new cloud physics parameterization in a large-eddy simulation model of marine stratocumulus. *Monthly Weather Review*, *128*(1), 229–243. https://doi.org/10.1175/1520-0493(2000)128<0229:ancppi>2.0.co;2

Minnis, P., Sun-Mack, S., Chen, Y., Chang, F. L., Yost, C. R., Smith, W. L., et al. (2021). CERES MODIS cloud product retrievals for Edition 4 - Part I: Algorithm changes. *IEEE Transactions on Geoscience and Remote Sensing*, *59*(4), 2744–2780. https://doi.org/10.1109/TGRS.2020.3008866

Morrison, H., & Milbrandt, J. A. (2015). Parameterization of cloud microphysics based on the prediction of bulk ice particle properties. Part I: Scheme description and idealized tests. *Journal of the Atmospheric Sciences*, *72*(1), 287–311. https://doi.org/10.1175/JAS-D-14-0065.1

Morrison, H., Curry, J. A., & Khvorostyanov, V. I. (2005). A new double-moment microphysics parameterization for application in cloud and climate models. Part I: Description. *Journal of the Atmospheric Sciences*, *62*(6), 1665–1677. https://doi.org/10.1175/JAS3446.1

Thompson, G., Field, P. R., Rasmussen, R. M., & Hall, W. D. (2008). Explicit forecasts of winter precipitation using an improved bulk microphysics scheme. Part II: Implementation of a new snow parameterization. *Monthly Weather Review*, *136*(12), 5095–5115. https://doi.org/10.1175/2008MWR2387.1

Yamaguchi, T., & Randall, D. A. (2008). Large-eddy simulation of evaporatively driven entrainment in cloud-topped mixed layers. *Journal of the Atmospheric Sciences*, *65*(5), 1481–1504. https://doi.org/10.1175/2007JAS2438.1